Narges Taheri* and Soheil Sayyahi

Effect of clay loading on the structural and mechanical properties of organoclay/HDI-based thermoplastic polyurethane nanocomposites

Abstract: Thermoplastic polyurethane/organically-modified montmorillonite (TPU/OMMT) nanocomposites were synthesized by the pre-polymer polymerization method using Cloisite® 30B organoclay, 1,6-hexamethylene diisocyanate (HDI), polycaprolactone diol (PCL diol, 2000 g/mol) and 1,4-butanediol (BDO). The hard segment content of the TPU was maintained at ~25.5% while the role of clay content was investigated at 1, 3 and 5 wt.% of clay concentration. The aim of this work was to obtain a high-performance polyurethane system while reaching a general microstructure-property relationship for TPU/OMMT nanocomposites. Clay exfoliation was achieved at 1 and 3 wt.% of clay loadings while some agglomerated clay sheets were observed in samples containing 5 wt.% OMMT. Significant hydrogen bonding occurred between the urethane linkages with unreacted -CH_2CH_2OH groups of the OMMT particles which resulted in strong matrix-filler interactions. Consequently, the values of tensile modulus were enhanced with clay content; namely a 177% improvement was observed for samples containing 5 wt.% OMMT. On the other hand, samples exhibited more thermoplastic behavior with the increase of clay content which resulted in lower deformability and lower values of tensile strength.

Keywords: clay content; degree of crystallinity; nanocomposites; organo-montmorillonite; thermoplastic polyurethane.

*Corresponding author: Narges Taheri, Department of Chemistry, Mahshahr Branch, Islamic Azad University, Mahshahr, Iran, e-mail: n.taheri99@gmail.com
Soheil Sayyahi: Department of Chemistry, Mahshahr Branch, Islamic Azad University, Mahshahr, Iran

1 Introduction

The smectite clays have been extensively used as reinforcing agents for preparation of polymer nanocomposites due to their various potential advantages (1–7). Clay nanoparticles at very low volume-fractions, can intensely improve the physio-mechanical properties of the final polymer system due to their light mass coupled with the high mechanical strength, high stiffness and high aspect ratio. Furthermore, clay minerals such as montmorillonite occur frequently in nature, thus can lower the often high cost of the polymer systems by reducing the amount of polymer used in the shaped structures. However, in order to achieve homogenous dispersion for small particles, clay minerals require further modification to overcome the inherent incompatibility of inorganic fillers with polymer chains. Fortunately, clays often exhibit a very rich intercalation chemistry, which allows them to be chemically modified and made compatible with organic polymers for dispersal on a nanometer length scale (8). Organically-modified montmorillonites (OMMT) are particularly gaining widespread interest due to their large aspect ratio and huge specific surface as much as 700 m^2/g (9), which are important factors in the significant improving of mechanical properties, as well as in avoiding the deterioration of impact strength, generally observed in microcomposites. The incorporation of organo-montmorillonite within thermoplastic polyurethanes (TPU) has become a prominent area of current research due to the outstanding mechanical properties, biocompatibility and versatility of polyurethane systems which makes TPU/OMMT nanocomposites interesting materials in the emerging field of nanoscience and particularly biomedical applications.

Many successful efforts (10–22) have been made to reinforce polyurethane with various loadings of organo-montmorillonites. Pattanayak and Jana (15) investigated the effect of clay loading on polyether and polyester-based polyurethane nanocomposites and concluded that the values of tensile strength, tensile modulus and elongation at break increased with clay content. Likewise, they observed that better dispersion of clay particles for

polyester-based nanocomposites containing 5 wt.% of organoclay, yielded much better improvement in tensile properties than its polyether-based nanocomposite counterpart. Zia et al. (22) studied the role of clay content on the chitin-bentonite polyurethane nanocomposites and found that clay incorporation improved the values of tensile strength up to 4 wt.% of clay content. However, a continuous decline in elongation at break was observed upon 1, 2, 4 and 8 wt.% of clay incorporation. Yao et al. (19) investigated the role of high clay loadings in PU/Na$^+$-modified montmorillonite nanocomposites and found similar trends for the values of tensile strength and elongation at break as in Pattanayak and Jana. Despite extensive attempts to correlate the microstructural interactions of clay-polymer matrix with the final mechanical properties of polyurethane nanocomposites, no established pattern has been found to describe the general microstructure-property relationships of TPU/OMMT nanocomposites.

In this work, high-performance thermoplastic polyurethanes containing PCL blocks as soft segment (SS) and HDI+BDO as hard segment (HS) were synthesized. A series of TPU/OMMT nanocomposites were achieved by incorporation of 1, 3 and 5 wt.% of a commercial organo-montmorillonite. The objective of the current study was to investigate the role of clay dispersion and clay-matrix interactions (in particular, the hydrogen bonding between clay particles and urethane linkages) on the degree of crystallinity, surface morphology and the final mechanical properties of TPU/OMMT nanocomposites.

2 Materials and methods

2.1 Materials

Thermoplastic polyurethanes were synthesized from a crystalline polyester-type polyol, an aliphatic diisocyanate, and a short chain diol as the chain extender. Polycaprolactone diol (PCL; average molecular weight M_n~2000 g/mol; melting temperature T_m=50°C; hydroxyl value of 51–63 mg KOH/g) was purchased from Sigma-Aldrich (St. Louis, MO, USA). The aliphatic diisocyanate used in this study was 1,6-hexamethylene diisocyanate (HDI; M_n=168.19 g/mol; NCO content=50 wt.%; linear formula OCN(CH$_2$)$_6$NCO) which was obtained from Sigma-Aldrich and 1,4-butanediol (BDO; M_n=90.12 g/mol; hydroxyl value=1245 mg KOH/g) was used as the chain extender and purchased from LyondellBasell (Rotterdam, Netherlands). The OMMT used in this study was a commercial clay (Cloisite® 30B; particle

size of 2–13 μm; layer thickness=1 nm; cation exchange capacity=0.9 meq/g) which was modified by methyl tallow bis-2-hydroxyethyl ammonium and purchased from Southern Clay Products Inc. (TX, USA)

2.2 Preparation of TPU/OMMT nanocomposites

Polyurethanes were synthesized by the pre-polymer polymerization process and with a 3:1:2 molar ratio of HDI, PCL diol and BDO (~25.5% hard segment content). A three-neck batch mixer, equipped with nitrogen inlet and a mechanical stirrer system was used to synthesize the pre-polymer. At first, a desired amount of PCL diol was introduced to the mixer and allowed to be melted at 60°C for 15 min. HDI was slowly added to the batch mixer and the pre-polymer was obtained from the reaction of PCL diol and HDI at 95°C for 2 h. To ensure that no NCO groups existed in the pre-polymer, di-n-butylamine titration method was carried out (see Table S1 in Supplementary Material for the NCO content of each sample). The chain extension reaction of TPU was completed by the reaction of 1 mol pre-polymer with 1 mol BDO at 85°C for 15 min. Before curing, the mixture was kept at 70°C and 15 Pa in a vacuum chamber for 15 min to degas. The mixed materials were then heated for 48 h at 80°C and kept at the room temperature for a minimum of 15 days before subsequent testing. Three sets of TPU/OMMT nanocomposites were obtained by incorporation of 1, 3 and 5 wt.% of Cloisite® 30B within the polyurethane matrix. During the pre-polymer process, desired amounts of Cloisite® 30B were added to the system and mixed with a propeller stirrer at 1000 rpm for 2 h. The amounts of -CH$_2$CH$_2$OH groups present in Cloisite® 30B clay were taken into consideration while balancing the molar ratio of -NCO and -OH groups to 1:1. To enhance the distribution level of clay particles in a polymeric matrix, ultrasonication is of particular interest and has been addressed in numerous reports (23–27). The ultrasonication process was performed at a frequency of 20 kHz with an inlet ultrasound power of around 1 W/ml (500hd Ultrasonic Processor, Aurizon Ultrasonics, LLC, WI, USA) for 30 min at 60°C in an external cooling bath. Further process conditions were the same as indicated for synthesizing the neat polyurethanes. The pristine thermoplastic polyurethane with approximately 25.5% of hard segments was simply coded as "TPU" and the prepared TPU/OMMT samples were coded as TPU-0X where "X" values are 1, 3 and 5 wt.% of the commercial organo-montmorillonite loaded to 100 wt.% of TPU matrix.

2.3 Characterization of TPU/OMMT nanocomposites

To evaluate the state of intercalation/exfoliation of organo-montmorillonite layers within the TPU matrix, wide-angle X-ray diffraction (WAXD) patterns of the virgin Cloisite® 30B particles and the TPU/OMMT nanocomposites with varying clay contents were carried out in the 2θ range of $2–10°$, using a high-resolution X-ray diffractometer (Bruker D8, Karlsruhe, Germany) which was equipped with a Nickel-filtered Cu Kα radiation ($\lambda=1.5406$ Å). The measurements were performed in a sealed tube at 40 kV, 40 mA and at scanning rate of $0.005°$ s^{-1}. Transmission electron microscopy (TEM) was also used to determine the state of clay dispersion in the polymer matrix. The nanocomposites were sectioned into ultra-thin slices (50–70 nm) at room temperature using a Leica UC7 ultramicrotome which was equipped with a diamond knife. High-resolution images were then attained using a JEM-2100 LaB6 microscope (JEOL, USA) with an accelerating voltage of 200 kV. To examine the completion of the polymerization reaction as well as to study the clay-polymer interactions in TPU/clay nanocomposites, Fourier-transform infrared spectroscopy (FT-IR) was carried out using a JASCO FT/IR-4000 spectrometer (Easton, USA). The IR spectra of Cloisite® 30B particles, the pristine TPU and TPU/clay nanocomposites were attained within the $4000–600$ cm^{-1} range and with a signal resolution of 2 cm^{-1}. The number average molecular weights (M_n) and the weight average molecular weights (M_w) of the pre-polymer, neat TPU and TPU/OMMT nanocomposites were determined by a Shimadzu (Kyoto, Japan) permeation chromatograph (GPC) calibrated with polystyrene standards. The operation temperature was 40°C. Tetrahydrofuran was used as eluent and elution rate was set at 0.5 ml/min. Differential scanning calorimetry (DSC) analysis was carried out using a DSC 203 F1 instrument (NETZSCH, Germany) under nitrogen atmosphere (gas flow 20 ml/min). The specimens were heated at a scanning rate of 10°C/min and a temperature range of 0–150°C. DSC thermograms were normalized to the mass fraction of the samples before analyzing. The surface morphology of nanocomposites was evaluated using high-magnification scanning electron microscopy (SEM, S-4160, Hitachi, equipped with an energy dispersive X-ray detector, Tokyo, Japan) at 20 kV. The specimens were coated with a thin gold layer of about 1–2 nm thickness by a Bal-Tec SCD-004 (LA, USA) sputtering equipment to prevent charging prior to imaging. The tensile properties (Young's modulus, tensile strength and elongation at break) of the TPU and TPU/OMMT nanocomposites were evaluated according to the test procedure of ASTM D 638 using a SANTAM (Model STM-20, Tehran, Iran) mechanical testing machine. Dumbbell type specimens for the tensile test were prepared using an appropriate punch. The test was performed at a constant crosshead speed of 20 mm/min and with a loading cell of 200 kgf.

3 Results and discussion

3.1 State of clay dispersion

Wide-angle X-ray diffraction (WAXD) was used to observe the extent of clay dispersion in the TPU nanocomposite samples. The WAXD patterns of the pure OMMT and TPU/clay nanocomposites are illustrated in Figure 1. Pure OMMT produced a sharp intense peak at $2\theta=4.78°$ which is related to the d-spacing of 18.48 Å of clay layers, according to Bragg's law ($d=\lambda/2\sin\theta$). The crystal structure of OMMT consists of two tetrahedral silicate sheets sandwiching a central octahedral sheet of aluminum hydroxide. Due to the weak dipolar or wan der Waals forces between clay stacks, polyurethane can easily enter into the interlayer spaces of clay platelets and push them far away. Exfoliation achieves when the interlayer spacing of clay layers exceeds the sensitivity of WAXD, thus the characteristic diffraction peaks are absent in exfoliated TPU/clay nanocomposites (17). For TPU nanocomposites containing 1 and 3 wt.% OMMT, no distinguishable reflections were observed, therefore suggesting the exfoliation of silicate layers in the polyurethane matrix. More detailed clay dispersion is shown by TEM micrographs of the cross-sectional views
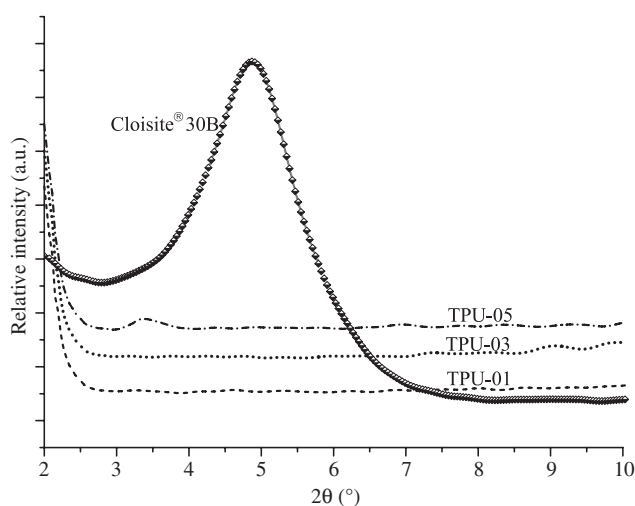

Figure 1: Wide-angle X-ray diffraction patterns of the pure Cloisite® 30B and TPU/clay nanocmposites containing 1, 3 and 5 wt.% of Cloisite® 30B in the 2θ range of 2–10°.
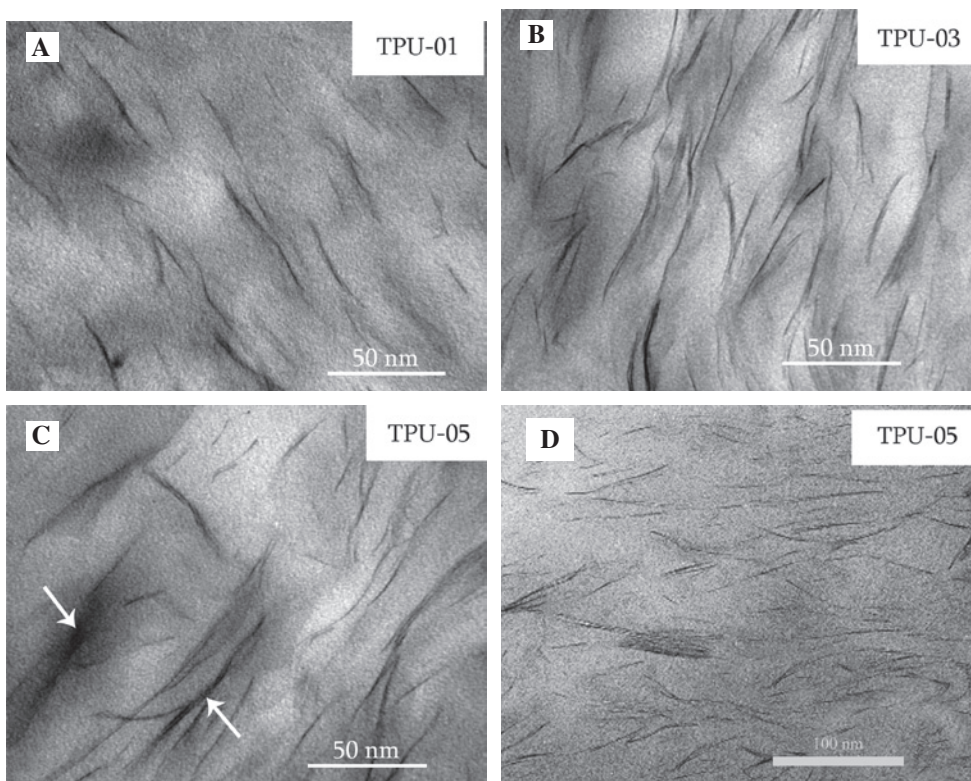
Figure 2: TEM images of TPU/OMMT nanocomposites at 50 nm for samples containing (A) 1 wt.%, (B) 3 wt.%, and (C) 5 wt.% Cloisite® 30B. Smaller magnification TEM image (100 nm) of the TPU-05 sample is shown in (D).

of TPU/clay nanocomposites in Figure 2A–D. Individual clay layers were observed as the prominent feature of the TPU-01 and TPU-03 cross-sections, supporting the results obtained from WAXD analysis. On the other hand, some agglomerated clay sheets were observed in TPU nanocomposites containing 5 wt.% OMMT as marked by white arrows in Figure 2C. Meanwhile, the overall individual scattering structure of the clay layers was still maintained, as can be seen in a smaller magnification TEM image of the TPU-05 sample (Figure 2D). Curiously enough, similar result was obtained for the WAXD pattern of the TPU-05 sample. It is evident from Figure 1 that TPU-05 revealed a broad peak at $2\theta=3.41°$ corresponding to 25.89 Å interlayer spacing. The shift of this peak to higher d-values (lower angles) compared to that of pure OMMT confirmed that the TPU chains were effectively introduced into the interlayers, leading to partially intercalated structure.

3.2 FTIR spectroscopy and gel permeation chromatography (GPC)

The FT-IR spectra of OMMT, pristine polyurethane and TPU/OMMT nanocomposites are depicted in Figure 3.

Organo-montmorillonite particles revealed (Figure 3A) characteristic absorption bands associated with the stretching of Si-O (1048 cm^{-1}) and the stretching of Al-Al-OH in the octahedral sheet of aluminum hydroxide (914 cm^{-1}) (16). Hydrocarbon chains of the organic ammonium ions in OMMT produced -CH vibrations at 2926, 2854 and 1470 cm^{-1} (13, 28). The asymmetric stretching vibration of structural -OH groups at 3632 cm^{-1} and hydrogen-bonded water bending band at 1633 cm^{-1} (13) were of particular interest as both structural -OH and water were capable of reacting with -NCO groups in isocyanate. For pristine TPU, the FT-IR was used mainly to evaluate the completion of polymerization reaction (Figure 3B). TPU showed 2948 and 2850 cm^{-1} (28) characteristic vibrations corresponding to the symmetric and asymmetric stretching of C-H groups. Most importantly, the absence of the -NCO band at 2250–2270 cm^{-1} (29) and the appearance of hydrogen-bonded and free carbonyl vibrations (1700 and 1732 cm^{-1}, respectively), as well as the hydrogen-bonded -NH band (3343 cm^{-1}) indicates that the urethane linkages were successfully formed (13, 28). The simultaneous detection of distinct free and hydrogen-bonded carbonyl groups was due to the remarkable phase separation of the polyurethane chain segments according to the
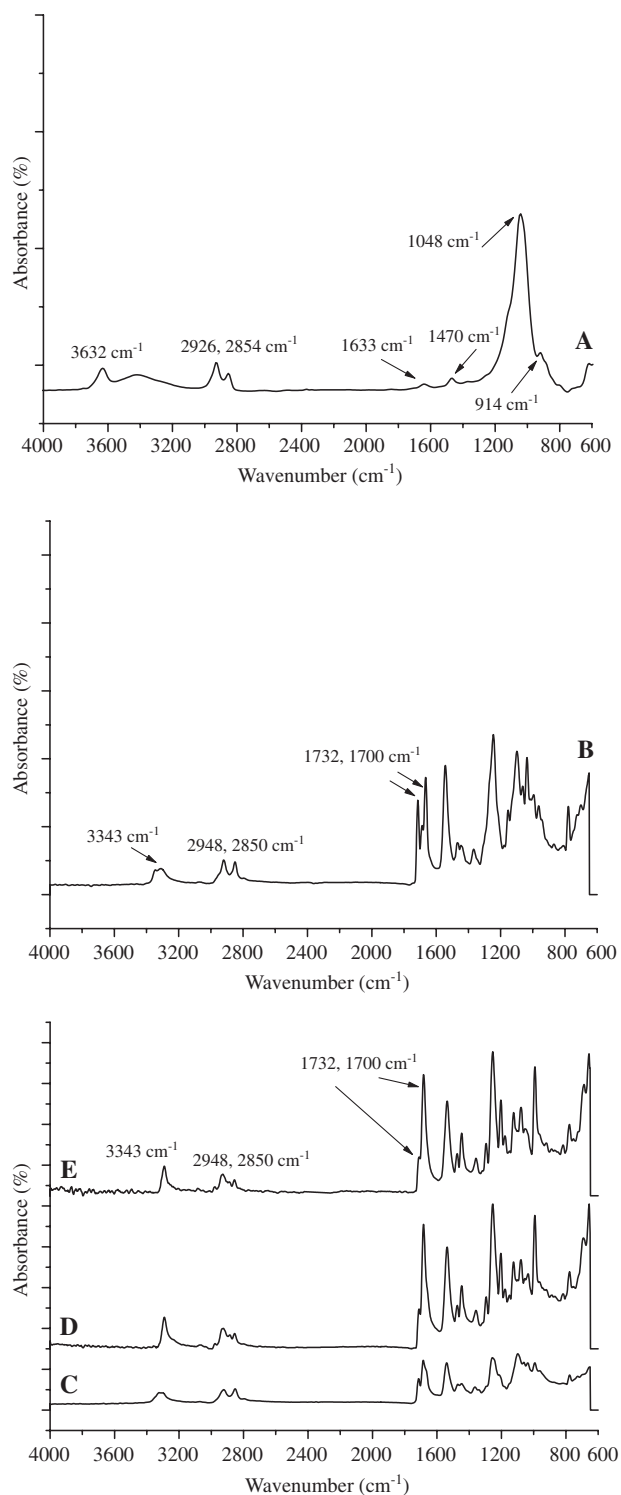
Figure 3: FT-IR spectra of (A) pure Cloisite® 30B, (B) pristine TPU, and TPU/OMMT nanocomposites containg 1, 3 and 5 wt.% of Cloisite® 30B (C–E, respectively).

literature (15). In terms of TPU/OMMT nanocomposites (Figure 3C–E), the main features of various bond vibrations remained the same as those of the pristine TPU. Note

that the free -OH band at 3622 cm^{-1} and hydrogen-bonded water bending peak at 1633 cm^{-1} in OMMT (see Figure 3A) were absent for the nanocomposite samples, indicating that strong interactions are occurring between -OH groups in organoclay and the -NCO groups in the isocyanate. By incorporation of only 1 wt.% organoclay within the TPU matrix, the intensity of the free carbonyl band at 1732 cm^{-1} decreased significantly. When clay loading increased to 3 and 5 wt.%, further reductions were observed in the intensity of the aforementioned vibration, indicating that the majority of carbonyl groups engaged in hydrogen bonding interactions. According to research (30), this was due to the hydrogen bonding between urethane free carbonyls with unreacted -CH$_2$CH$_2$OH groups in quaternary ammonium ions on the OMMT particles. Likewise, the relative intensity of the hydrogen-bonded -NH band at 3343 cm^{-1} increased (see Figure 3D,E) with clay loading, verifying the results obtained from WAXD and TEM tests in regard to the occurrence of strong interactions between the filler-matrix interface.

The GPC results of the number average molecular weight (M_n), the weight average molecular weight (M_w) and the polydispersity index (PDI=M_w/M_n) for different samples are obtained (see Figure S1a,b in Supplementary Material). A value of 4825 g·mol^{-1} was calculated for the M_n of the pre-polymer. The relatively high molecular weight of the pre-polymer was due to the employed PCL diol, which reportedly tends to yield higher molecular weights compared to polyether-type polyols (30). As expected, the values of M_n and M_w increased significantly upon the chain extension reaction. In particular, a 538% increase was observed for the M_n of the pristine TPU compared to the pre-polymer. For nanocomposite samples, the M_w values increased meaningfully with clay content, despite the constant ratio of NCO/OH (hard segment content). This could be attributed to the viscosity of the chain segments, which progressively increased owing to the presence of solid clay particles.

3.3 Differential scanning calorimetry (DSC)

In order to examine the degree of crystallinity, the DSC heating curves of the neat TPU and TPU/OMMT nanocomposites were acquired (see Figure S2 in Supplementary Material). All curves exhibited melting endothermic peaks at the temperature range of 25–50°C, which can be attributed to the he crystallization melting of the PCL diol in the TPU matrix. The crystallinity of the soft segments (X_c) can be calculated according to the following equation:

$$X_c = \frac{\Delta H_m}{\Delta H_f^*} \quad\quad [1]$$

where ΔH_m is the normalized melting enthalpy of the PCL diol soft segments and ΔH_f^* is the specific heat of melting of a pure semicrystalline PCL macrodiol (77.4 J·g⁻¹) (30). As shown by the crystallinity measurements in Table 1, the TPU-01 sample showed increased crystallinity compared to the neat TPU. This was due to the nucleating effect of the OMMT particles, which imposed additional crystalline structure to the soft chain segments of the nanocomposite sample. However, by further increase of the clay content,

the degree of crystallinity declined. This was expected, since the phase separation between the soft and hard segments can be greatly diminished in the presence of clay particles. Furthermore, the melting transition temperatures (T_m) of the nanocomposites shifted slightly to higher temperatures with clay increasing content, owing to the presence of solid OMMT particles.

3.4 Morphology

The surface morphology of the pristine TPU and TPU/OMMT nanocomposites containing different clay loadings was examined by high-resolution SEM micrographs. Meanwhile, the corresponding silicon mapping images of the nanocomposites were acquired to visually assess the distribution level of clay particles on the specimens' surfaces. The most prominent feature of the pristine polyurethane's surface was a coarse structure (see Figure 4A), which could be attributed to the large extent of phase separation between the soft and hard segments in the TPU sample (31). Additionally, polyurethane systems which are obtained from aliphatic diisocyanates (e.g. HDI and IPDI) tend to give a rougher surface morphology than

Table 1: Characteristic parameters of the differential scanning calorimetry (DSC) analysis.

Sample code	ΔH_m (J/g)	X_c (%)	T_m (°C)
TPU	21.0	27.1	37.5
TPU-01	22.2	28.7	38.5
TPU-03	17.9	23.1	39
TPU-05	14.5	18.7	40

ΔH_m, melting enthalpy of soft segments.
X_c, crystallinity of soft segments.
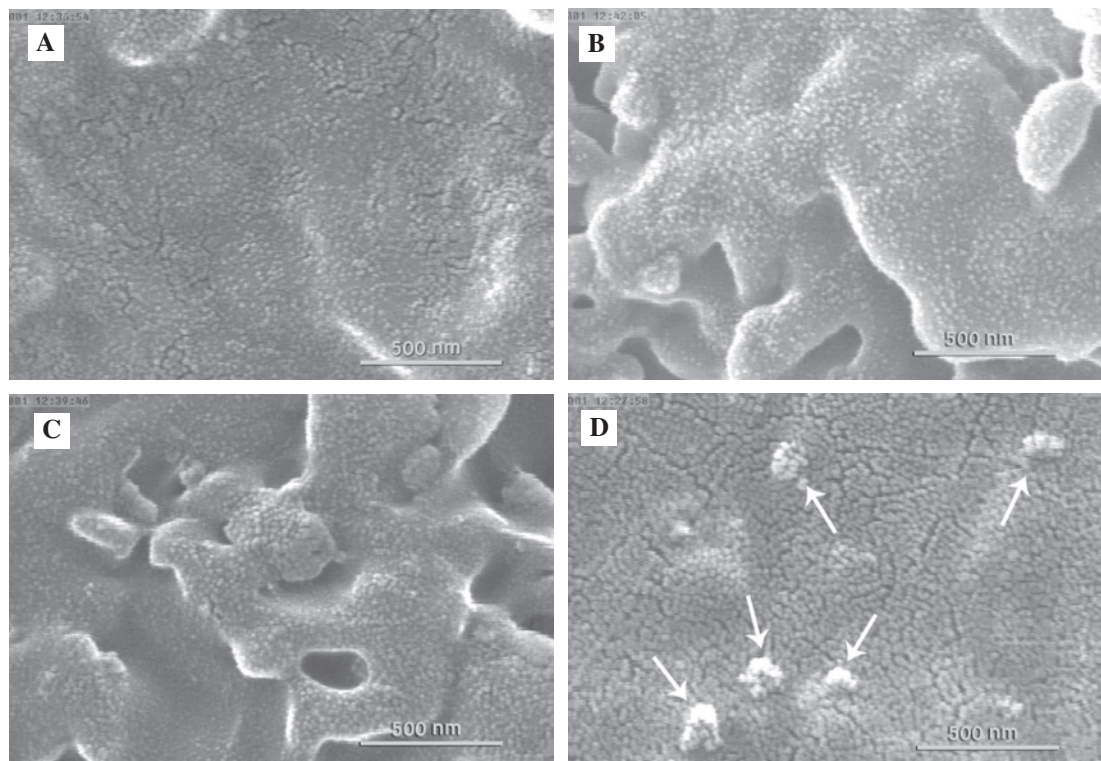T_m, melting point of soft segments.

Figure 4: SEM micrographs at magnification of 500 nm for (A) pristine TPU, and TPU/OMMT nanocomposites containg 1, 3 and 5 wt.% of Cloisite® 30B (B–D, respectively).

that of aromatic-based PUs (such as those based on MDI) (31, 32), which further explains the spherulitic grain-like structure of the TPU surface. SEM images of the TPU/clay nanocomposites showed that organo-montmorillonite particles were dispersed to the scale of single particles, particularly at clay loadings of 1 and 3 wt.% (Figure 4B,C). The results of the EDS Si mapping further revealed (see Figure S3a–c in Supplementary Material) that OMMT particles were evenly distributed and mostly scattered on the scale of single particles. At 3 wt.%, the spherulites grew together and formed interconnected spherulitic structure, which is addressed in other reports by the possible nucleating effect of organoclay (33). Self-assembled texture in the form of microclusters was observed for nanocomposite containing 5 wt.% OMMT. The presence of these microclusters (marked by white arrows in Figure 4D) confirmed that some agglomerated organoclay particles are present in TPU-05 and that OMMT acted partially as a nucleating agent.

3.5 Mechanical properties

Mechanical properties of the pristine TPU and TPU/OMMT nanocomposites were evaluated using tensile testing. Typical stress-strain diagrams of the pristine TPU and its clay nanocomposites are depicted in Figure 5 and the values of Young's modulus, tensile strength and elongation at break are presented in Table 2. All samples exhibited linear elastic behavior at low strain region ($\varepsilon<50\%$) and plastic deformation at higher strain regions. The pristine TPU showed excellent Young's modulus with a relatively low hard segment content. Because of the proposed
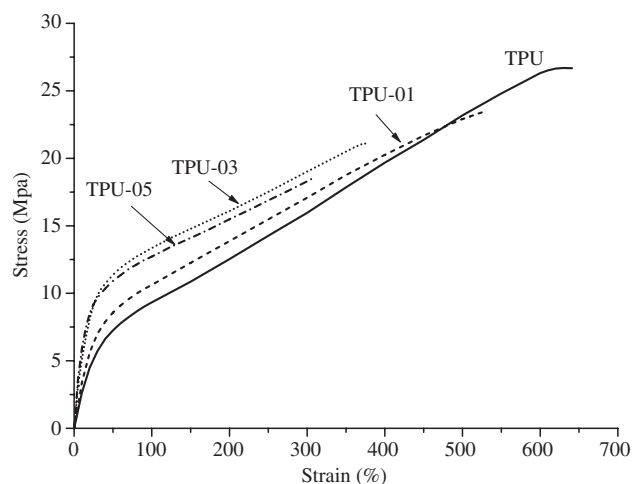
Table 2: Tensile properties of the pristine TPU and its OMMT nanocomposites.

Sample	Tensile modulus (MPa)±standard deviation	Tensile strength (MPa)±standard deviation	Elongation at break (%)±standard deviation
TPU	26±0.66	27±0.80	641±18
TPU-01	34 ±1.04	23±0.47	527±16
TPU-03	63±1.87	21±0.63	377±11
TPU-05	73±2.31	19±0.52	309±10

phase separated microstructure, HDI-based polyurethane systems exhibit superior mechanical properties compared to the typical MDI-based PUs (32). As a general trend, higher tensile modulus were achieved for nanocomposites with higher clay contents. Adding only 1 wt.% of organoclay led to a 28% increase in the Young's modulus. At 3 and 5 wt.% of clay loading, immense improvements of about 140 and 177% were observed for the Young's modulus compared to the pristine TPU, respectively. Tien and Wei (34) attributed such enhancement of the tensile modulus to the better interfacial bonding between the reactive organoclay and polymer chains. Thus, clay particles acted as reinforcing agents in TPU, with the interlayer having high tensile modulus. By increasing clay concentration, in addition to the increase of interfacial interaction of polymer, the reinforcing property of organoclay itself may contribute to the enhancement of tensile modulus of TPU. On the other hand, the values of tensile strength and elongation at break declined with clay content. As clearly seen from the stress-strain diagrams in Figure 5, nanocomposite specimens shifted toward more thermoplastic behavior with the increase of clay content, i.e. the samples showed less flexibility with significant upturn in the slope of elastic region. This was due to the homogenous dispersion of clay particles in the high-concentration soft chain segments which are responsible for the overall flexibility of PU systems. Consequently, TPU/OMMT nanocomposites reveal higher tensile modulus and lower deformability with the increase of clay content.

4 Conclusions

The mechanical properties of TPU/OMMT nanocomposites can be correlated with the state of clay dispersion in the polyurethane matrix, the microstructural filler-matrix interactions (specifically the possible hydrogen bonding between functional -OH groups of the organoclay with the urethane linkages) and the surface morphology of

Figure 5: Stress-strain diagrams of the pure TPU and its clay nanocomposites containing 1, 3 and 5 wt.% Cloisite® 30B.

the nanocomposites. Exfoliation of clay silicate layers in the polymer matrix showed to be a prominent factor in the improvement of tensile modulus, although relative agglomerated particles seem to be inevitable in high clay loadings due to the high surface energy of the clay particles. The free -OH vibration at 3622 cm^{-1} and hydrogen-bonded water bending band at 1633 cm^{-1} in OMMT disappeared in the IR spectra of nanocomposites, indicating strong interactions between clay platelets and urethane linkages. Furthermore, the prominent coarse texture of the surface morphology suggested that large extent of phase separation occurred within the polymer matrix which may be the prime reason of the outstanding mechanical properties achieved for the pristine TPU and its clay nanocomposites.

References

1. Puffr R, Špátová JL, Brožek J. Clay mineral/polyamide nanocomposites obtained by in-situ polymerization or melt intercalation. Appl Clay Sci. 2013;83–84:294–9.
2. Shokrieh MM, Kefayati AR, Chitsazzadeh M. Fabrication and mechanical properties of clay/epoxy nanocomposite and its polymer concrete. Mater Design. 2012;40:443–52.
3. Sadeghipour H, Ebadi-Dehaghani H, Ashouri D, Mousavian S, Hashemi-Fesharaki M, Shahbazi Gahrouei M. Effects of modified and non-modified clay on the rheological behavior of high density polyethylene. Compos Part B-Eng. 2013;52:164–71.
4. Zapata PA, Belver C, Quijada R, Aranda P, Ruiz-Hitzky E. Silica/clay organo-heterostructures to promote polyethylene-clay nanocomposites by *in situ* polymerization. Appl Catal A-Gen. 2013;453:142–50.
5. Nam B-U, Min K-D, Son Y. Investigation of the nanostructure, thermal stability, and mechanical properties of polylactic acid/cellulose acetate butyrate/clay nanocomposites. Mater Lett. 2015;150:118–21.
6. Wan C, Qiao X, Zhang Yo, Zhang Yi. Effect of different clay treatment on morphology and mechanical properties of PVC-clay nanocomposites. Polym Test 2003;22:453–61.
7. Suin S, Maiti S, Shrivastava NK, Khatua BB. Mechanically improved and optically transparent polycarbonate/clay nanocomposites using phosphonium modified organoclay. Mater Design. 2014;54:553–63.
8. Mondal M, Chattopadhyay PK, Chattopadhyay S, Setua DK. Thermal and morphological analysis of thermoplastic polyurethane-clay nanocomposites: Comparison of efficacy of dual modified laponite vs. commercial montmorillonites. Thermochim Acta. 2010;510:185–94.
9. Wu Z, Zhou C, Zhu N. The nucleating effect of montmorillonite on crystallization of nylon 1212/montmorillonite nanocomposite. Polym Test 2002;21:479–83.
10. Rehab A, Salahuddin N. Nanocomposite materials based on polyurethane intercalated into montmorillonite clay. Mater Sci Eng A. 2005;399:368–76.
11. Barick AK, Tripathy DK. Thermal and dynamic mechanical characterization of thermoplastic polyurethane/organoclay nanocomposites prepared by melt compounding. Mater Sci Eng A. 2010;527:812–23.
12. Cao X, Lee LJ, Widya T, Macosko C. Polyurethane/clay nanocomposites foams: processing, structure and properties. Polymer 2005;46:775–83.
13. Heidariana M, Shishesaz MA, Kassiriha SM, Nematollahi M. Characterization of structure and corrosion resistivity of polyurethane/organoclay nanocomposite coatings prepared through an ultrasonication assisted process. Prog Org Coat. 2010;68:180–8.
14. Hooghten RV, Gyssels S, Estravis S, Rodriguez-Perez MA, Moldenaers P. Understanding the effect of particle surface free energy on the structural and mechanical properties of clay-laden rigid polyurethane foams. Eur Polym J. 2014;60:135–44.
15. Pattanayak A, Jana SC. Thermoplastic polyurethane nanocomposites of reactive silicate clays: effects of soft segments on properties. Polymer 2005;46:5183–93.
16. Jang ES, Bahadar Khan S, Seo J, Nam YH, Choi WJ, Akhtar K, Han H. Synthesis and characterization of novel UV-curable polyurethane-clay nanohybrid: Influence of organically modified layered silicates on the properties of polyurethane. Prog Org Coat. 2011;71:36–42.
17. Pauzi NNPN, Majid RA, Dzulkifli MH, Yahya MY. Development of rigid bio-based polyurethane foam reinforced with nanoclay. Compos Part B-Eng. 2014;67:521–6.
18. Salahuddin N, Abo-El-Enein SA, Selim A, El-Dien OS. Synthesis and characterization of polyurethane/organo-montmorillonite nanocomposites. Appl Clay Sci. 2010;47:242–8.
19. Yao KJ, Song M, Hourston DJ, Lou DZ. Polymer/layered clay nanocomposites: 2 polyurethane nanocomposites. Polymer 2002;43:1017–20.
20. Sarier N, Onder E. Organic modification of montmorillonite with low molecular weight polyethylene glycols and its use in polyurethane nanocomposite foams. Thermochim Acta. 2010;510:113–21.
21. Moon S-Y, Kim J-k, Nah C, Lee Y-S. Polyurethane/montmorillonite nanocomposites prepared from crystalline polyols, using 1,4-butanediol and organoclay hybrid as chain extenders. Eur Polym J. 2004;40:1615–21.
22. Zia KM, Zuber M, Barikani M, Hussain R, Jamil T, Anjum S. Cytotoxicity and mechanical behavior of chitin−bentonite clay based polyurethane bio-nanocomposites. Int J Biol Macromol. 2011;49:1131–6.
23. Lam C-k, Lau K-t, Cheung H-y, Ling H-y. Effect of ultrasound sonication in nanoclay clusters of nanoclay/epoxy composites. Mater Lett. 2005;59:1369–72.
24. Liang K, Shi S.Q. Nanoclay filled soy-based polyurethane foam. J Appl Polym Sci. 2011;119:1857–63.
25. Isik I, Yilmazer U, Bayram G. Impact modified epoxy/montmorillonite nanocomposites: synthesis and characterization. Polymer 2003;44:6371–7.
26. Bensadoun F, Kchit N, Billotte C, Trochu F, Ruiz E. A comparative study of dispersion techniques for nanocomposite made with nanoclays and an unsaturated polyester resin. J Nanomater. 2011;2011:1–12.

27. Heidarian M, Shishesaz MR, Kassiriha SM, Nematollahi M. Study on the effect of ultrasonication time on transport properties of polyurethane/organoclay nanocomposite coatings. J Coat Tech Res. 2011;8:265–274.

28. Barrioni BR, de Carvalho SM, Oréfice RL, de Oliveira AAR, de Magalhães Pereira M. Synthesis and characterization of biodegradable polyurethane films based on HDI with hydrolyzable crosslinked bonds and a homogeneous structure for biomedical applications. Mat Sci Eng C-Mater. 2015;52:22–30.

29. Thakur S, Karak N. Castor oil-based hyperbranched polyurethanes as advanced surface coating materials. Prog Org Coat. 2013;76:157–64.

30. Cao F, Jana SC. Nanoclay-tethered shape memory polyurethane nanocomposites. Polymer 2007;48:3790–800.

31. Prisacariu C. Polyurethane Elastomers: From Morphology to Mechanical Aspects. Chapter 2: Structural Studies on Polyurethane Elastomers, 2011. Edition: 2011th, Springer, NewYork.

32. Fernández-d'Arlas B, Khan U, Rueda L, Coleman JN, Mondragon I, Corcuera MA, Eceiza A. Influence of hard segment content and nature on polyurethane/multiwalled carbon nanotube composites. Compos Sci Technol. 2011;71:1030–8.

33. Barick AK, Tripathy DK. Effect of organically modified layered silicate nanoclay on the dynamic viscoelastic properties of thermoplastic polyurethane nanocomposites. Appl Clay Sci. 2011;52:312–21.

34. Tien YI, Wei KH. Hydrogen bonding and mechanical properties in segmented montmorillonite/polyurethane nanocomposites of different hard segment ratios. Polymer 2001;42:3213–21.